Intracellular transport by motor proteins with the same directionality

Kewei Xie, and Qian Wang ✉

Department of Physics, University of Science and Technology of China, Hefei 230026, China

✉Correspondence: Qian Wang, E-mail: wqq@ustc.edu.cn

Graphical abstract

Two kinesins on the microtubule.

Public summary

- We establish a theoretical framework to study transport by motors with the same directionality by combining simulation and analytical derivation.

- Stronger binding between motors and microtubules leads to stronger cooperation between motors.

- We introduce a deep learning method by which the motor parameters can be easily identified for expected transport features.

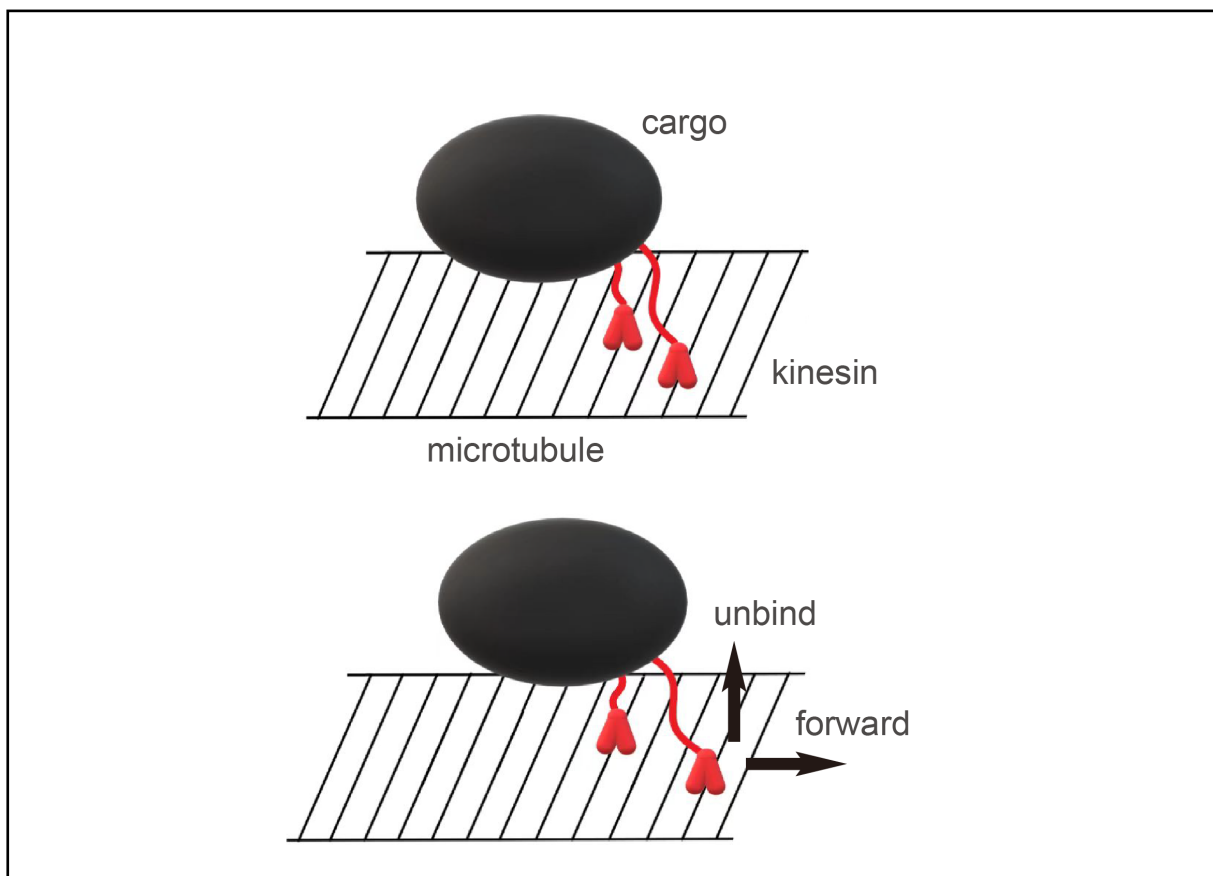# Intracellular transport by motor proteins with the same directionality

Kewei Xie, and Qian Wang ✉

Department of Physics, University of Science and Technology of China, Hefei 230026, China

✉Correspondence: Qian Wang, E-mail: wqq@ustc.edu.cn

Abstract: Active intracellular transport is mainly performed by a group of special nanomachines called motor proteins. During transport, cooperation between motor proteins significantly influences important transport features, such as distance and velocity. To understand this mechanism, we combine Gillespie simulation and analytical derivation to demonstrate how the mechanical properties of a single motor influence the cooperation between multiple motors, further regulating the transport distance. In addition, we build a deep learning model to help us quickly obtain the motor parameters. Our results shed light on the physical nature of intracellular transport by motor proteins with the same directionality.

Keywords: motor protein; intracellular transport; deep learning

CLC number: Q51   **Document code:** A

1 Introduction

Motor proteins utilize energy from ATP hydrolysis to perform intracellular transport[1−4], an essential biological function in cells. Transport interference due to motor protein disorder can cause a variety of neurodegenerative diseases[5−6]. Therefore, understanding the physics of transport continues to draw attention in the field[7].

Intracellular transport is usually performed by two types of motor proteins, kinesins and dyneins[8]. Kinesins walk toward the plus end of the microtubule, and dyneins walk toward the minus end[9]. Due to the opposite directionalities of carriers, cargo frequently moves bidirectionally[10−11]. Thus, to understand this process, a large number of theoretical studies focus on modeling cargo simultaneously transported by kinesins and dyneins[7, 12−15]. The most successful work is the tug-of-war (TOW) model developed by the Lipowsky lab[13]. The model well describes the competition between motors arising from opposite directionalities by reproducing previous in vitro experimental data[16]. However, in vivo experiments indicate that there is also cooperation between kinesins and dyneins, which the TOW model fails to explain[17]. This so-called "codependent paradox" is solved by the competition and cooperation (CC) model developed in our previous work[18]. By using the CC model, we reproduced the in vivo experimental measurements[14] with high accuracy. In addition, the analytical solution of the transport distance was derived to uncover the physical nature of competition and cooperation[18].

Although the CC model has gained success, it still has two limitations. First, in cells, the cargo is carried by multiple kinesins and multiple dyneins. To establish a complete theory of intracellular transport, we should focus on not only the correlation between kinesins and dyneins but also that between motors with the same directionality. This part is missing in

our previous work[18]. Second, the CC model utilizes a number of motor parameters as input. It is typically very difficult to find suitable parameters that lead to experimental transport features, as it is a multidimensional fitting problem. The TOW model has a similar problem.

We overcome these limitations in this work. First, by combining simulation and analytical derivation, a theoretical framework was established to study transport by motors with the same directionality. Second, we introduced a deep learning (DL) model by which the motor parameters can be efficiently identified for expected transport features. To increase the generality of the DL model, it was trained not only for motors with the same directionality but also for motors with opposite directionality. Our work is an important supplement and optimization of the previous research contents.

2 Methods

2.1 Computational model

We used the discrete stochastic model in our previous work[18] to describe intracellular transport by multiple motors. In the absence of force, each motor moves along the microtubule with the step size l_0. The forward velocity is v_0. The backward velocity is ignored because it is much smaller than the forward velocity[13]. Meanwhile, each motor stochastically detaches from the microtubule track with the unbinding rate ε_0 and rebinds to the track with the binding rate π_0.

Each motor connects to the cargo by an elastic spring with elastic coefficient k. Therefore, mechanical forces will be generated if the distance between any motor and the cargo increases. Assuming that the position of the cargo is x_c, the position of the motors is $\{x_1, x_2, \cdots\}$ and the maximum number of motors is N, the mechanical force exerted on motor i, F_i, can

be calculated as

$$F_i = kl_0(x_i - x_c),\qquad(1)$$

$$x_c = \frac{k\sum_{i=1}^{N}x_i}{kN}.\qquad(2)$$

In the presence of force, the forward velocity follows a simplified version of the original TOW model[13]:

$$v(F) = \begin{cases} v_0\left(1 - \dfrac{F}{F_s}\right), & F \leqslant F_s; \\ 0, & F > F_s. \end{cases}\qquad(3)$$

Here, the forward velocity decreases linearly with F. When F reaches or exceeds the stall force F_s, the forward velocity decreases to zero. Meanwhile, the unbinding rate also increases exponentially with F:

$$\varepsilon(F) = \varepsilon_0 e^{\frac{|F|}{F_d}}.\qquad(4)$$

The binding rate π_0 of any motor does not change with F, indicating that motors always bind to the microtubule in a relaxed state.

In summary, each motor is described by six parameters: the forward velocity v_0, the unbinding rate ε_0, the binding rate π_0, the stall force F_s, the detachment force F_d and the elastic coefficient k. The values of those parameters are shown in Table 1. All trajectories were simulated by the Gillespie algorithm[19].

2.2 Deep learning model

We developed a DL model to identify the motor parameters that can reconstruct the key transport feature. The parameter set of a transport system was represented by a 14-dimensional vector $[v_0^K, v_0^D, \pi_0^K, \pi_0^D, \varepsilon_0^K, \varepsilon_0^D, F_s^K, F_s^D, F_d^K, F_d^D, k^K, k^D, N^K, N^D]$. Here, N represents the motor numbers, and the superscript K (D) represents the kinesin (dynein) motor. N^K and N^D were set to nonnegative integers, and other parameters were nonnegative. The feature set was represented by a 4-dimensional vector [proportion of pause, pause duration, positive runlength, and negative runlength]. The element of the vector represents the proportion of pause time in total time, the average time per pause, the runlength of positive transport and the runlength of negative transport. Please see the detailed definitions in our previous work[18].

To train the DL model, first, we randomly picked a parameter set and measured the corresponding transport features

Table 1. Parameters used in the paper.

Unbinding rate ε_0 (s^{-1})	1[20-21]
Binding rate π_0 (s^{-1})	5[22]
Stall force F_s (pN)	6[20, 23]
Detachment force F_d (pN)	3[20]
Stiffness k (pN/nm)	0.2[24]
Step size l_0 (nm)	8[24-25]
Forward velocity v_0 (nm/s)	1000[21, 25]

by Gillespie simulations. This calculation was repeated 10^4 times in the following space: $v_0 \in [160 \text{ nm/s}, 4000 \text{ nm/s}]$, $\pi_0 \in [0.6 \text{ s}^{-1}, 15 \text{ s}^{-1}]$, $\varepsilon_0 \in [0.12 \text{ s}^{-1}, 3 \text{ s}^{-1}]$, $F_s \in [0.6 \text{ pN}, 15 \text{ pN}]$, $F_d \in [0.36 \text{ pN}, 9 \text{ pN}]$, $k \in [0.02 \text{ pN/nm}, 0.5 \text{ pN/nm}]$, $N \in [2, 8]$. Next, we trained a fully connected network to establish the connection between the motor parameters and the transport features. A rectified linear unit (ReLU) was chosen as the activation function. We chose two hidden layers with 700 nodes for each layer.

To test the accuracy of this DL model, first, we randomly picked an expected feature set M_1 and predicted the corresponding motor parameters by the DL model. Next, Gillespie simulations with the predicted parameters were performed to measure the actual transport features M_2. The error of the DL model was defined $\frac{|M_2 - M_1|}{M_1}$. This calculation was repeated 10^3 times in the following space: proportion of pause $\in [5\%, 40\%]$, pause duration $\in [0.1 \text{ s}, 1 \text{ s}]$, positive runlength $\in [100 \text{ nm}, 1000 \text{ nm}]$, negativer unlength $\in [100 \text{ nm}, 1000 \text{ nm}]$.

3 Results and discussion

3.1 Transport distance influenced by motor parameters

We first studied how various motor parameters influenced the overall transport distance S (defined as the distance from the initial position to where all motors detach from the moving track). For convenience, in this work, we only considered the case with two kinesins unless otherwise stated (Fig. 1a). Each kinesin could either (i) move forward on the microtubule, (ii) unbind from the microtubule, or (iii) bind to the microtubule.

The simulation results indicate that S increases with the binding rate π (Fig. 1b) and the detachment force F_d
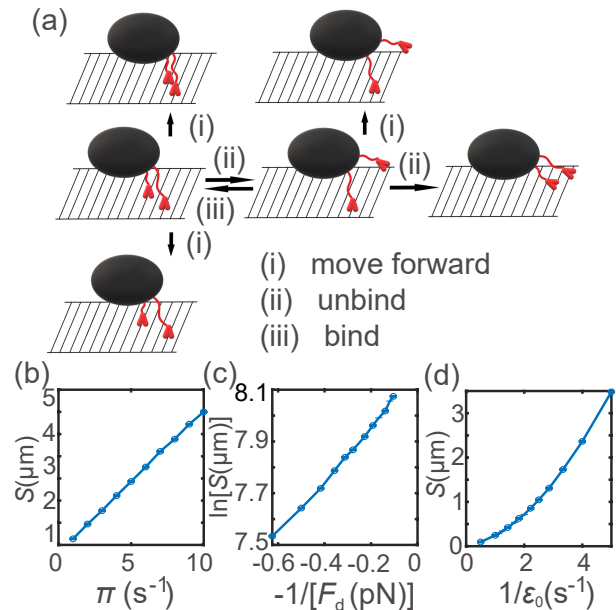
Fig. 1. (a) Schematic illustration of transport by two kinesins. Each kinesin can move stochastically in three modes: (i) moving forward; (ii) unbinding and (iii) binding. (b) The overall transport distance S as a function of the binding rate π. (c) $\ln S$ as a function of e^{-1/F_d}, where F_d is the detachment force. (d) S as a function of $1/\varepsilon_0$, where ε_0 is the detachment rate.

(Fig. 1c). It is qualitatively understandable. When the velocity remains unchanged, S should be proportional to the residence time of the motors on the microtubule, which increases with π or F_d (Eq. (2)). In contrast, S decreases with the detachment rate ε_0 (Fig. 1d), as a higher ε_0 shortens the residence time.

Simulations provide a convenient way to establish the relation between S and motor parameters. The physical nature of those relations is still elusive. For example, why does S increase linearly with the binding rate (Fig. 1b) but nonlinearly with the detachment force (Fig. 1c)? To solve this issue, we derive the analytical expression of S in the next section.

3.2 Analytical expression of the transport distance

The motion of the two kinesins was modeled as the transitions among three states: (I) two kinesins binding to the microtubule, (II) one kinesin binding to the microtubule, and (III) no kinesin binding to the microtubule. In each transition, the displacement of cargo is $S_i (i = 1, 2, 3)$, and the probability is $P_i (i = 1, 2, 3)$. Here, $P_1 = 1$, $P_2 + P_3 = 1$, and $S_2 = S_3$.

Assuming that $P(x)$ is the probability of having transition (II)→(I) repeated x times in one complete transport, $P(x)$ and the corresponding transport distance, $S(x)$, can be respectively calculated as

$$P(x) = (P_1 P_2)^x P_3, \qquad (5)$$

$$S(x) = x(S_1 + S_2) + (S_1 + S_3). \qquad (6)$$

The expectation value of the total transport S is

$$S = \sum_{x=0}^{\infty} P(x) S(x) = \frac{1}{P_3} (S_1 + S_3). \qquad (7)$$

For a single kinesin, its residence time on the microtubule is $1/\varepsilon_0$, and the average velocity is v_0. We can further calculate S_2, S_3, P_2, P_3 as

$$P_2 = \frac{\pi_0}{\varepsilon_0 + \pi_0}, \quad P_3 = \frac{\varepsilon_0}{\varepsilon_0 + \pi_0}, \quad S_2 = S_3 = \frac{v_0}{\varepsilon_0} \frac{\varepsilon_0 + \pi_0}{\varepsilon_0}. \qquad (8)$$

Combining Eqs. (7) and (8), we obtain

$$S = \left(1 + \frac{\pi_0}{\varepsilon_0}\right) S_1 + \frac{v_0}{\varepsilon_0} = \gamma S_1 + S_0. \qquad (9)$$

Note that $S_0 = \dfrac{v_0}{\varepsilon_0}$ represents the transport distance if the transport is only performed by one single kinesin; therefore, Eq. (9) indicates that the transport distance with two kinesins is always γS_1 longer than that with a single kinesin. The accuracy of Eq. (9) is validated by a perfect match (R^2=0.999) between the analytical calculation and simulation results (Fig. 2b).

The exact analytical form of S_1 is complicated. Therefore, we made an approximation that two kinesins walk alternately. Under this circumstance, when the leading kinesin walks one step on the microtubule, there is an elastic tension $F = kl_0$ between two kinesins. Here, l_0 is the step size. Correspondingly, the detachment rate of the two kinesins changes from ε_0 to $\varepsilon_1 = \varepsilon_0 e^{kl_0/F_d}$, the velocity of the leading kinesin changes from v_0 to 0, and the velocity of the trailing kinesin changes
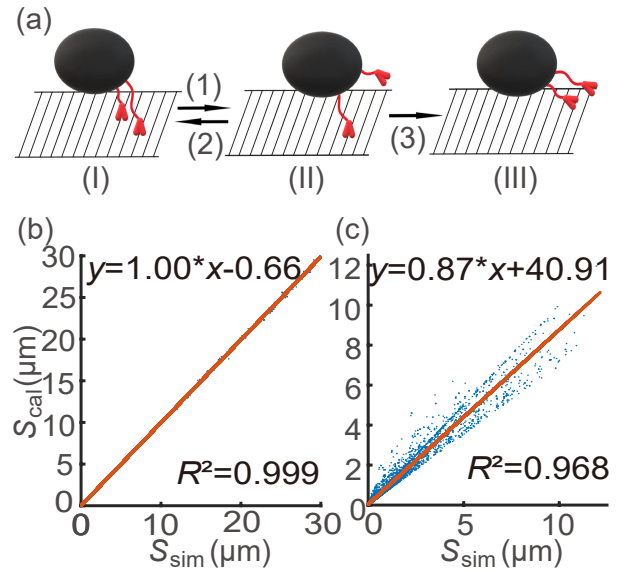
Fig. 2. (a) Three states during transport carried by two kinesins. (b) Comparison of the transport distance S calculated by Eq. (9) and by simulations from the CC model. The input parameter is a 6-dimensional vector $(v_0, \pi_0, \varepsilon_0, F_s, F_d, k)$. We repeat the calculation 10^4 times by randomly picking in the following parameter space: $v_0 \in [160 \text{ nm/s}, 4000 \text{ nm/s}]$, $\pi_0 \in [0.6 \text{ s}^{-1}, 15 \text{ s}^{-1}]$, $\varepsilon_0 \in [0.12 \text{ s}^{-1}, 3 \text{ s}^{-1}]$, $F_s \in [0.6 \text{ pN}, 15 \text{ pN}]$, $F_d \in [0.36 \text{ pN}, 9 \text{ pN}]$, and $k \in [0.02 \text{ pN/nm}, 0.5 \text{ pN/nm}]$. (c) Comparison of S_1 calculated by Eq. (12) and by simulations from the CC model. R represents the correlation coefficient.

from v_0 to $v_1 = v_0(1 + kl_0/F_s)$. Assuming that the probability of the leading kinesin walking m steps before unbinding from the microtubule is $p(m)$, we can calculate $p(m)$ as

$$p(m) = \begin{cases} \left(\dfrac{v_0/l_0}{v_0/l_0 + \varepsilon_0} \dfrac{v_1/l_0}{v_1/l_0 + 2\varepsilon_1}\right)^m \left(\dfrac{2\varepsilon_1}{v_1/l_0} + \dfrac{\varepsilon_0}{v_0/l_0 + \varepsilon_0}\right), & m > 0; \\[2ex] \dfrac{\varepsilon_0}{v_0/l_0 + \varepsilon_0}, & m = 0. \end{cases} \qquad (10)$$

Considering that the position of cargo approximately equals the position of the leading motor, S_1 can be written as

$$S_1 = \sum_{m=0}^{\infty} m p(m) l_0 = \frac{(v_1/l_0 + 2\varepsilon_1) v_0}{2\varepsilon_1 v_0 + \varepsilon_0 v_1 + 2\varepsilon_0 \varepsilon_1 l_0}. \qquad (11)$$

Substituting Eq. (11) into Eq. (9), we obtain

$$S = \left(1 + \frac{\pi_0}{\varepsilon_0}\right) S_1 + \frac{v_0}{\varepsilon_0} = \left(1 + \frac{\pi_0}{\varepsilon_0}\right) \frac{(v_1/l_0 + 2\varepsilon_1) v_0}{2\varepsilon_1 v_0 + \varepsilon_0 v_1 + 2\varepsilon_0 \varepsilon_1 l_0} + \frac{v_0}{\varepsilon_0}. \qquad (12)$$

In realistic biologic situations, $v_i \gg \varepsilon_i$. Therefore, S_1 can be approximated as

$$S_1 \approx \frac{1}{\dfrac{2\exp(kl_0/F_d)}{(1 + kl_0/F_s)} + 1} \frac{v_0}{\varepsilon_0}. \qquad (13)$$

Substituting Eq. (13) into Eq. (9), we have

$$S = \left(1 + \frac{\pi_0}{\varepsilon_0}\right) S_1 + \frac{v_0}{\varepsilon_0} = \left(\frac{\frac{\pi_0}{\varepsilon_0} + 1}{\frac{2\exp(kl_0/F_{\mathrm{d}})}{(1 + kl_0/F_{\mathrm{s}})} + 1} + 1\right)\frac{v_0}{\varepsilon_0}. \quad (14)$$

The accuracy of Eq. (12) is validated by a great match ($R^2 = 0.968$) between the analytical calculation and simulation results (Fig. 2c). In addition, Eq. (14) indicates that S linearly increases with the binding rate π_0, exponentially increases with $-1/F_{\mathrm{d}}$, and quadratically increases with $1/\varepsilon_0$. This is consistent with Fig. 1b–d.

For one kinesin with one dynein, the transport distance was derived as[18]

$$S = \lambda^{\mathrm{D \to K}} \frac{v_0^{\mathrm{K}}}{\varepsilon_0^{\mathrm{K}}} - \lambda^{\mathrm{K \to D}} \frac{v_0^{\mathrm{D}}}{\varepsilon_0^{\mathrm{D}}}. \quad (15)$$

Here, the superscript K (D) represents the parameters of kinesin (dynein), and λ are the correlation factors. More details can be found in our previous work[18]. The case with multiple kinesins and dyneins will be studied in the future.

3.3 Error analysis

To derive Eqs. (12) and (14), we assumed that two kinesins walk alternately. However, one kinesin can walk two steps in a row, leading to discrepancies between the analytical calculation and the simulation shown in Fig. 2c. Therefore, it is necessary to analyze when this assumption is valid and how much the error (defined as $\eta = |S_{\mathrm{cal}} - S_{\mathrm{sim}}|/S_{\mathrm{sim}}$. S_{cal} is the analytical calculation, and S_{sim} is the simulation result) is.

The assumption of alternate walking has two consequences. First, after the leading kinesin makes one forward step, it is forced to wait until the trailing kinesin catches up, which slows down the averaged velocity of the whole system. As a result, Eq. (12) underestimates the transport distance. This is consistent with the fact that the slope of the fitting equation in Fig. 2c is 0.87 instead of 1. This is error type I.

Second, under this assumption, the maximum separation between two kinesins is restrained to one step size l_0, which is shorter than the real case when the separation can be $2l_0$, $3l_0$, etc. This approximation results in an underestimated averaged intermotor tension. Based on Eq. (4), in this case, the residence time would be overestimated, as would the transport distance. This is error type II.

These two consequences have opposite effects. They intertwine and cause the accuracy of Eq. (12) to change with the intermotor tension (or equivalently, the elastic coefficient k) in a nonmonotonic way. The largest error appears in the absence of intermotor tension F, where the analytical calculation is smaller than the simulation value (Fig. 3a, b, $k = 0$). Error I quickly drops with increasing k, while error II increases instead. As a result, the overall error first decreases and then increases (Fig. 3a). Meanwhile, the analytical calculation gradually becomes larger than the simulation value (Fig. 3b). When k is sufficiently large, the overall error decreases again (Fig. 3b), as the intermotor tension F reduces the probability of the leading kinesin having two continuous steps by decreasing its velocity based on Eq. (3). Noticeably, Eq. (4) indicates that when the detachment force $F_{\mathrm{d}} \to \infty$, the detachment rate is insensitive to intermotor tensions. Under
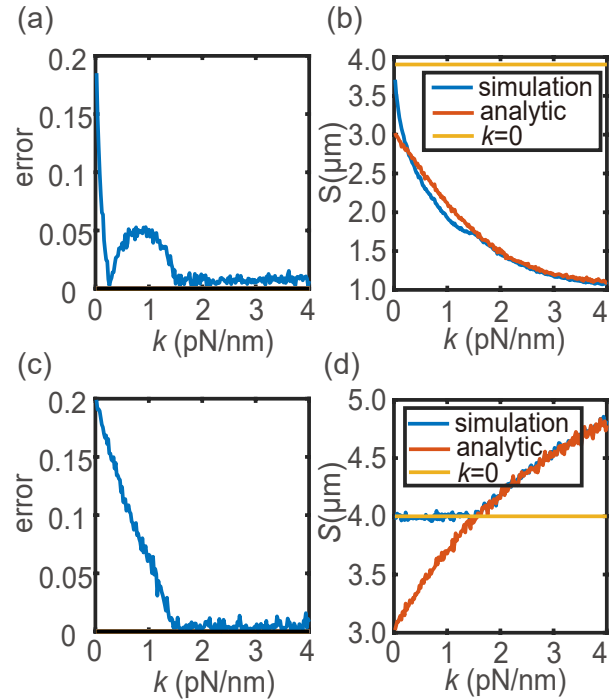
Fig. 3. (a) Error between the simulation and analytical calculation by Eq. (12) as a function of the elastic coefficient of kinesin, k. We define the error as $\eta = |S_{\mathrm{cal}} - S_{\mathrm{sim}}|/S_{\mathrm{sim}}$. (b) The distance S decays with the spring constant k. The blue line represents the Gillespie simulation result. The orange line represents the analytical result calculated by Eq. (12). The yellow line represents the analytical result calculated by Eq. (18). (c) and (d) are the same as (a) and (b) but the detachment force $F_{\mathrm{d}} \to \infty$.

this circumstance, type II error disappears. Then, the overall error decreases monotonically with the elastic coefficient k, as indicated by Fig. 3c, d.

We can calculate the largest error of Eq. (12), i.e., when the elastic coefficient k is zero. Assume that the displacement of one kinesin is m and another kinesin is n. Predictably, m and n must appear symmetrically. In this way, following the previous method, we can write the displacement change S_1 and the probability $P_1(m, n)$ of the progress from state I to state II (Fig. 2a).

$$P_1(m, n) = \left(\frac{v_0/l_0}{2v_0/l_0 + 2\varepsilon_0}\right)^{m+n} \frac{\varepsilon_0}{v_0}, \quad (16)$$

$$S_1 = \sum_{m=0}^{\infty} \sum_{n=0}^{\infty} \frac{m+n}{2} P_1(m, n) l_0 = \frac{v_0}{2\varepsilon_0}. \quad (17)$$

As before, we substitute S_1 into the expression S to obtain

$$S = \left(1 + \frac{\pi_0}{\varepsilon_0}\right) S_1 + \frac{v_0}{\varepsilon_0} = \left(\frac{3}{2} + \frac{\pi_0}{2\varepsilon_0}\right)\frac{v_0}{\varepsilon_0}. \quad (18)$$

Comparing Eq. (18) and Eq. (12) at $k = 0$, we obtain the maximum error of Eq. (12):

$$\eta = \frac{1}{9}\left(1 + \frac{2}{3\varepsilon_0/\pi_0 + 1}\right). \quad (19)$$

The error η is negatively correlated with ε_0 and positively correlated with π_0. When $\varepsilon_0 = 0$ or $\pi_0 = \infty$, η reaches its maxim-

um value of 1/3. In previous experiments, k was found to be 0.2 pN/nm for kinesin[24] and 0.05 pN/nm[26] for dynein. In this region, η is smaller than 0.05, indicating that our approximation of alternative walking is valid (Fig. 3a).

3.4 Correlation between two motors

If two motors do not interfere with each other and are completely independent, the transport distance in this case should be twice that with a single motor, $S = 2S_0$. However, the correlation between these two motors usually causes $S = \lambda S_0$. Eq. (14) shows that the correlation coefficient λ is

$$\lambda = \frac{\dfrac{\pi_0}{\varepsilon_0} + 1}{\dfrac{2\exp(kl_0/F_d)}{(1 + kl_0/F_s)} + 1} + 1. \tag{20}$$

Note that the binding free energy of a motor protein to the microtubule can be represented as $\Delta G = -k_B T \ln \dfrac{\pi_0}{\varepsilon_0}$; therefore, ΔG is the inherent parameter that dictates whether two motor proteins are cooperative ($\lambda > 2$) or noncooperative ($\lambda < 2$), T is the temperature of the environment. The cooperative region requires $\lambda > 2$, which gives

$$\Delta G < [\ln\left(1 + \frac{kl_0}{F_s}\right) - \ln 2 - \frac{kl_0}{F_d}]k_B T. \tag{21}$$

Stronger binding between motors and microtubules leads to stronger cooperation between motors.

In the extreme case of $k = 0$ (no intermotor tension), Eq. (14) should be replaced with Eq. (18). Under this circumstance, the correlation coefficient λ is $\left(\dfrac{3}{2} + \dfrac{\pi_0}{2\varepsilon_0}\right)$. Therefore, the separatrix between cooperative and noncooperative regions will be simplified to $\Delta G = 0$.

3.5 Deep learning model

To match the simulation data with the experimental data, we need to optimize the motor parameters in the model. This procedure was finished by the DL model in Fig. 4a.

There are three factors affecting the accuracy of the DL model: the number of training steps, the size of the training set and the complexity of the neural network, such as the number of hidden layers and neurons. To reduce the error as much as possible, we adjusted the above parameters to determine the best setting, and the results are shown in Fig. 4b–d.

First, the model has the minimum error when the training step equals 1500 (Fig. 4b). Excessive training leads to overfitting. Second, the model has better performance at two hidden layers than at one layer and three layers (Fig. 4c). In addition, the error reaches the minimum when there are 700 nodes for each layer. Finally, the error decreases as the training set increases (Fig. 4d). After testing those parameters of the DL model, we finally chose two hidden layers with 700 nodes for each layer.

We evaluated the DL model on the testing set. The average error is 14%, and the probability of having an error less than 20% is 85% (Fig. 4e). The run length has the largest error, as it is the most sensitive to input parameters. To show the ad-
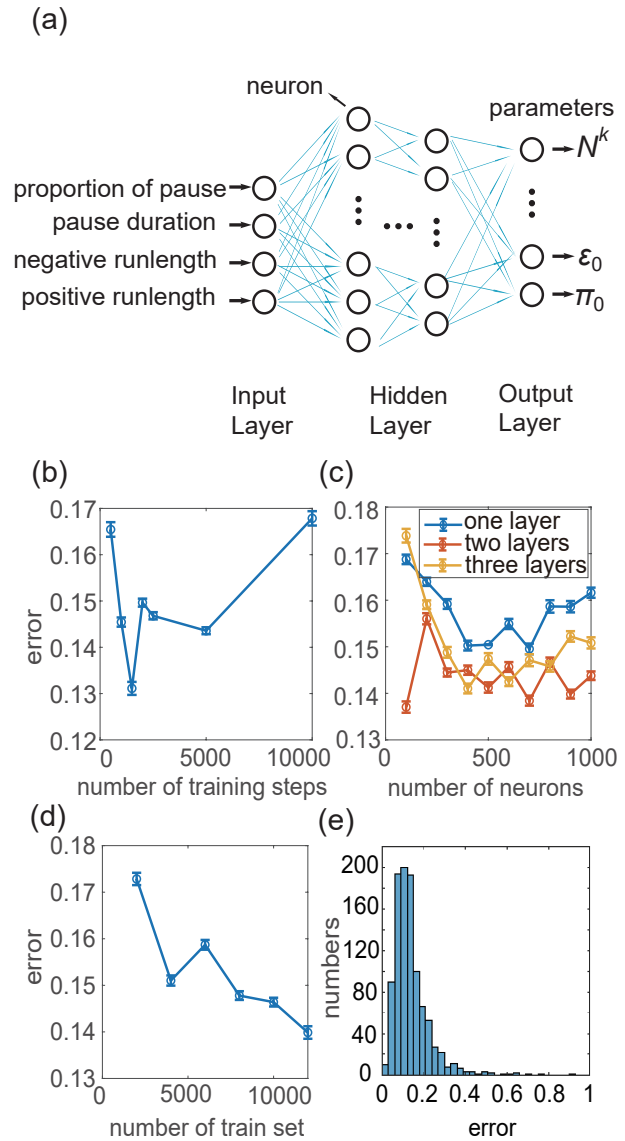
Fig. 4. (a) Deep learning neural network architecture. (b) The error of the deep learning changed by the number of training steps. (c) The error changed by the number of neurons and layers of the neural network. (d) The error changed by the size of the training set. (e) The distribution of errors.

vantage of our method, on the same testing set, we also calculated the error by using the widely used gradient descent (GD) method[27]. The GD method gains an averaged error of 62% after 20000 cycles (taking 3 d), much more inaccurate (62% versus 14% for the averaged error) and much more time consuming (3 d versus 3 s) than the DL model.

There are two ways to further improve the prediction. First, if we add two extra inputs in the DL model: the interval between pauses and the reverse probability after pause, the proportion of data with errors less than 10% can increase from 36% to 55%. Second, if we use the DL model to obtain an initial guess of the input parameter, then followed by the GD method, the averaged error can be reduced from 14% to 6% after 100 cycles of GD.

4 Conclusions

In this work, we established a theoretical framework to study intracellular transport by motor proteins with the same directionality. The central finding is that the binding free energy of a single motor to the microtubule dictates the cooperation between multiple motors. A lower free energy causes a longer transport distance. For a simple system (two motors), an explicit analytical solution was derived to calculate the transport distance. More complicated systems can be well described by a discrete stochastic model in which the parameters are identified by a deep learning neural network. Our work provides new insights to intracellular transport by motor proteins. In the future, we will extend the system to multiple motors with opposite directionalities.

Acknowledgements

Conflict of interest

The authors declare that they have no conflict of interest.

Biographies

Kewei Xie   is a graduate student under the tutelage of Prof. Qian Wang at the University of Science and Technology of China. His research focuses on the transport by motor proteins.

Qian Wang   is a Professor at the University of Science and Technology of China. He received his Ph.D. degree from the University of Houston in 2012. His research focuses on developing analytical and theoretical tools to understand physical rules behind biological phenomena.

References

[1] Vale R D. The molecular motor toolbox for intracellular transport. *Cell,* **2003**, *112*: 467–480.

[2] Cross R A, McAinsh A. Prime movers: The mechanochemistry of mitotic kinesins. *Nature Reviews Molecular Cell Biology,* **2014**, *15*: 257–271.

[3] Kolomeisky A B, Fisher M E. Molecular motors: A theorist's perspective. *Annual Review of Physical Chemistry,* **2007**, *58*: 675–695.

[4] Hirokawa N, Noda Y, Okada Y. Kinesin and dynein superfamily proteins in organelle transport and cell division. *Current Opinion in Cell Biology,* **1998**, *10*: 60–73.

[5] Rath O, Kozielski F. Kinesins and cancer. *Nature Reviews Cancer,* **2012**, *12*: 527–539.

[6] Millecamps S, Julien J P. Axonal transport deficits and neurodegenerative diseases. *Nature Reviews Neuroscience,* **2013**, *14*: 161–176.

[7] Veigel C, Schmidt C F. Moving into the cell: Single-molecule studies of molecular motors in complex environments. *Nature Reviews Molecular Cell Biology,* **2011**, *12*: 163–176.

[8] Pilling A D, Horiuchi D, Lively C M, et al. Kinesin-1 and dynein are the primary motors for fast transport of mitochondria in *Drosophila* motor axons. *Molecular Biology of the Cell,* **2006**, *17*: 2057–2068.

[9] Kural C, Kim H, Syed S, et al. Kinesin and dynein move a peroxisome in vivo: A tug-of-war or coordinated movement. *Science,* **2005**, *308*: 1469–1472.

[10] Gross S P. Hither and yon: A review of bi-directional microtubule-based transport. *Physical Biology,* **2004**, *1*: R1–R11.

[11] Welte M A. Bidirectional transport along microtubules. *Current Biology,* **2004**, *14*: R525–R537.

[12] Kozielski F, Sack S, Marx A, et al. The crystal structure of dimeric kinesin and implications for microtubule-dependent motility. *Cell,* **1997**, *91*: 985–994.

[13] Müller M J I, Klumpp S, Lipowsky R. Tug-of-war as a cooperative mechanism for bidirectional cargo transport by molecular motors. *Proceedings of the National Academy of Sciences of the United States of America,* **2008**, *105*: 4609–4614.

[14] Kunwar A, Tripathy S K, Xu J, et al. Mechanical stochastic tug-of-war models cannot explain bidirectional lipid-droplet transport. *Proceedings of the National Academy of Sciences of the United States of America,* **2011**, *108*: 18960–18965.

[15] Vu H T, Chakrabarti S, Hinczewski M, et al. Discrete step sizes of molecular motors lead to bimodal non-Gaussian velocity distributions under force. *Physical Review Letters,* **2016**, *117*: 078101.

[16] Vale R D, Malik F, Brown D. Directional instability of microtubule transport in the presence of kinesin and dynein, two opposite polarity motor proteins. *Journal of Cell Biology,* **1992**, *119*: 1589–1596.

[17] Hancock W O. Bidirectional cargo transport: Moving beyond tug of war. *Nature Reviews Molecular Cell Biology,* **2014**, *15*: 615–628.

[18] Xie K, Wang Q. Cooperation and competition coexist in bidirectional transport by motor proteins. *The Journal of Physical Chemistry Letters,* **2022**, *13*: 7336–7341.

[19] Gillespie D T. Exact stochastic simulation of coupled chemical-reactions. *Journal of Physical Chemistry,* **1977**, *81*: 2340–2361.

[20] Schnitzer M J, Visscher K, Block S M. Force production by single kinesin motors. *Nature Cell Biology,* **2000**, *2*: 718–723.

[21] Vale R D, Funatsu T, Pierce D W, et al. Direct observation of single kinesin molecules moving along microtubules. *Nature,* **1996**, *380*: 451–453.

[22] Leduc C, Campàs O, Zeldovich K B, et al. Cooperative extraction of membrane nanotubes by molecular motors. *Proceedings of the National Academy of Sciences of the United States of America,* **2004**, *101*: 17096–17101.

[23] Svoboda K, Block S M. Force and velocity measured for single kinesin molecules. *Cell,* **1994**, *77*: 773–784.

[24] Rogers A R, Driver J W, Constantinou P E, et al. Negative interference dominates collective transport of kinesin motors in the absence of load. *Physical Chemistry Chemical Physics,* **2009**, *11*: 4882–4889.

[25] Carter N J, Cross R A. Mechanics of the kinesin step. *Nature,* **2005**, *435*: 308–312.

[26] Oiwa K, Sakakibara H. Recent progress in dynein structure and mechanism. *Current Opinion in Cell Biology,* **2005**, *17*: 98–103.

[27] Avriel M. Nonlinear Programming: Analysis and Methods. Englewood Cliffs, NJ: Prentice-Hall, **1976**.